THE ASTRONOMICAL JOURNAL, 120:1426–1435, 2000 September

CHANDRA X-RAY OBSERVATORY STUDY OF THE ORION NEBULA CLUSTER AND BN/KL REGION

GORDON GARMIRE,[1] ERIC D. FEIGELSON,[1] PATRICK BROOS,[1] LYNNE A. HILLENBRAND,[2] STEVEN H. PRAVDO,[3] LEISA TOWNSLEY,[1] AND YOHKO TSUBOI[1]
Received 2000 March 27; accepted 2000 May 30

ABSTRACT

About 1000 X-ray emitting young pre–main-sequence (PMS) stars distributed in mass from $\sim 0.05\ M_\odot$ brown dwarfs to a $\sim 50\ M_\odot$ O star are detected in an image of the Orion Nebula obtained with the Advanced CCD Imaging Spectrometer on board the *Chandra X-Ray Observatory*. This is the richest field of sources ever obtained in X-ray astronomy. Individual X-ray luminosities in the Orion Nebula cluster range from the sensitivity limit of 2×10^{28} ergs s^{-1} to $\sim 10^{32}$ ergs s^{-1}. ACIS sources include 85%–90% of $V < 20$ stars, plus a lower but substantial fraction of deeply embedded stars with extinctions as high as $A_V \simeq 60$. The relationships between X-ray and other PMS stellar properties suggest that X-ray luminosity of lower-mass PMS stars depends more on mass, and possibly stellar rotation, than on bolometric luminosity, as widely reported. In a subsample of 17 unabsorbed stars with mass $\simeq 1\ M_\odot$, X-ray luminosities are constant at a high level around $L_x \simeq 2 \times 10^{30}$ ergs s^{-1} for the first $\simeq 2$ Myr while descending the convective Hayashi track, but diverge during the 2–10 Myr phase with X-ray emission plummeting in some stars but remaining high in others. This behavior is consistent with the distribution of X-ray luminosities on the zero-age main sequence and with current theories of their rotational history and magnetic dynamos.

The sources in the Becklin-Neugebauer/Kleinman-Low region of massive star formation are discussed in detail. They include both unabsorbed and embedded low-mass members of the Orion Nebula cluster, the luminous infrared Source n, and a class of sources without optical or infrared counterparts that may be new magnetically active embedded PMS stars. Several X-ray sources are also variable radio emitters, an association often seen in magnetically active PMS stars. Faint X-ray emission is seen close to, but apparently not coincident with, the Becklin-Neugebauer object. Its nature is not clear.

Key words: infrared radiation — ISM: individual (Orion Nebula) — stars: activity — stars: pre–main-sequence — X-rays

1. INTRODUCTION

X-ray emission among pre–main-sequence (PMS) stars with masses $M \lesssim 2\ M_\odot$ is known to be elevated 10^1 to $> 10^4$ times above typical main-sequence levels (Feigelson & Montmerle 1999). High-amplitude X-ray variability and hard spectra, supported by multiwavelength studies, indicate that the emission is in most cases due to solar-type magnetic flares, where plasma is heated to high temperatures by violent reconnection events in magnetic loops. However, the empirical relationships between PMS X-ray emission and stellar age, mass, radius, and rotation are complex (see e.g., Feigelson et al. 1993) and their links to astrophysical theory are not strong. For example, if surface magnetic activity is a manifestation of a simple rotation-driven magnetic dynamo in the stellar interior and if current theories about the evolution of angular momentum in PMS stars hold (Bouvier, Forestini, & Allain 1997), then specific predictions about the evolution of the X-ray luminosity function during the PMS phase can be tested if sufficiently large samples are obtained. X-rays are known to be produced in high-mass star formation regions, but little is known about the structure or astrophysical origins of this emission (Churchwell 1999).

The largest sample of PMS stars observable in a single field is the Orion Nebula cluster (ONC). The OB members of the ONC illuminate the Orion Nebula (= Messier 42), a blister H II region at the near edge of the Orion A giant molecular cloud. The ONC is a nearby stellar cluster and one of the densest PMS clusters known, with $\simeq 2000$ members concentrated in a 1 pc (8′) radius sphere and with 80% of the stars younger than 1 My (Hillenbrand 1997). It was the first star-forming region to be detected in the X-ray band (Giacconi et al. 1972), and nonimaging studies soon found the X-ray emission is extended on scales of a parsec or larger (den Boggende et al. 1978; Bradt & Kelley 1979). Early explanations for the Orion X-rays included winds from the massive Trapezium stars colliding with each other or the molecular cloud and hot coronae or magnetic activity in lower mass T Tauri stars. The Einstein (Ku & Chanan 1979), ROSAT (Gagné, Caillault, & Stauffer 1995; Geier, Wendker, & Wisotzki 1995; Alcalá et al. 1996) and ASCA (Yamauchi et al. 1996) imaging X-ray observatories established that both the Trapezium stars and many lower-mass T Tauri stars contribute to the X-ray emission.

These studies could detect only a modest fraction of the ONC stars because of the high stellar concentration and heavy absorption by molecular material along the line of sight. NASA's *Chandra X-Ray Observatory* launched on 1999 July 23 with its Advanced CCD Imaging Spectrometer (ACIS) detector provides an unprecedented combination of

[1] Department of Astronomy and Astrophysics, 525 Davey Laboratory, Pennsylvania State University, University Park, PA 16802.
[2] Department of Astronomy, MS 105-24, California Institute of Technology, Pasadena, CA 91125.
[3] Jet Propulsion Laboratory, MS 306-438, 4800 Oak Grove Drive, Pasadena, CA 91109.

capabilities—a wide spectral bandpass, $<1''$ spatial resolution, very low cosmic-ray and detector background levels, and moderate spectral resolution at every pixel—that make it particularly well-suited to the study of crowded and absorbed clusters of faint X-ray sources.

After describing the data in § 2, we discuss demographics of PMS stellar X-ray emission (§ 3). The next sections describe two of many possible investigations of this rich data set: in § 4 we examine the evolution of magnetic activity in solar-mass stars, and in § 5 we present the X-ray sources from stars in the Becklin-Neugebauer/Kleinman-Low (BN/KL) star forming region in OMC 1. Later papers will provide a more comprehensive analysis of this and additional observations of the Orion Nebula (Feigelson et al. 2000).

2. OBSERVATIONS AND DATA ANALYSIS

The ONC was observed with the ACIS-I array detector on board the *Chandra X-Ray Observatory* (Weisskopf, O'Dell, & van Speybroeck 1996) for 47.8 ks on 1999 October 12. The array consists of four abutted charge-coupled devices (CCDs) specially designed for X-ray studies (Garmire et al. 2000[4]). Two chips from the ACIS-S spectroscopic array were also turned on, but their data will not be discussed here. Starting with Level 1 processed event lists provided by the pipeline processing at the Chandra X-Ray Center, we removed several types of CCD events likely dominated by particles rather than imaged X-rays: energies above 8 and below 0.2 keV; split events except for ASCA grades 0, 2, 3, 4, and 6; cosmic-ray events causing stripes along amplifier nodes; hot columns and other low-quality flagged events. The aim point on chip I3 was $5^{h}35^{m}15\overset{s}{.}0$ $-5°23'20''$.

The resulting image (Fig. 1) shows hundreds of sources concentrated around the bright Trapezium stars. Several instrumental effects are also evident, such as the broadening of the point response function off-axis because of the telescope optics, the $11''$ gaps between the CCD chips blurred by the satellite aspect dither, and the trailing of events from the brightest sources due to events arriving during the chip

[4] Detailed descriptions of the ACIS instrument and its operation can be found at http://www.astro.psu.edu/xray/docs/sop and http://www.astro.psu.edu/xray/docs/cal_report.

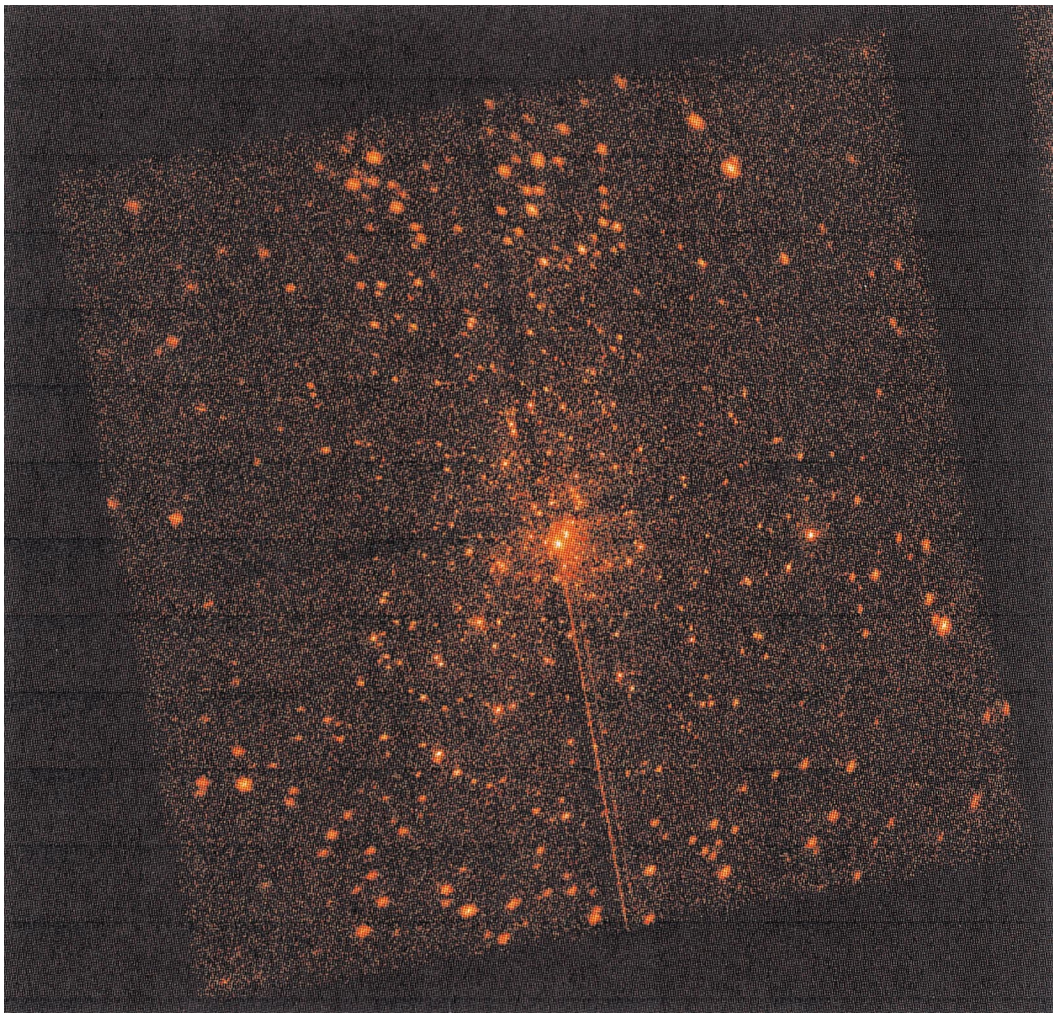

FIG. 1.—ACIS-I image of the Orion Nebula Cluster in the 0.2–8 keV band showing $\simeq$1000 X-ray sources. The $17' \times 17'$ array is shown here at reduced resolution with $2'' \times 2''$ pixels. The massive O7 star θ^1C Ori is the brightest source near the center. Here and in Fig. 2, colors are scaled to the logarithm of the number of events in each pixel. Pixels with no events are black, those with individual events are dark red, and those with multiple events are scaled logarithmically. North is at top, and east to the left.

readout. The brightest Trapezium sources also suffer photon pileup, which distorts their morphology, flux, and spectrum.

An additional problem in the current data set is the degradation of charge transfer efficiency of the ACIS-I CCDs due to high dosage of particle irradiation early in the *Chandra* mission (Prigozhin et al. 2000). Corrective measures were taken to arrest the degradation as soon as it was discovered and data acquired after 2000 January 29 should have a reduced problem because of changes in on-board operation of the detector to mitigate charge transfer inefficiency. Improved data processing techniques have been developed to treat this problem (Townsley et al. 2000) and are applied in our analysis in § 5. The results of other portions of the study should not be seriously affected by the charge transfer degradation.

The excellent point-spread function produced by the *Chandra* mirrors and the satellite aspect solution, combined with the very low background rate in the detector, permits the detection of sources as weak as $\simeq 7$ photons and the resolution of sources as closely spaced as 2″. This high sensitivity and resolution is illustrated in Figure 2. For a weakly absorbed ONC star with a typical PMS thermal spectrum with energy $kT = 1$ keV (see Preibisch 1997), a limit of 7 photons corresponds to a flux of 9×10^{-16} ergs s^{-1} cm^{-2} (0.2–8 keV) or, assuming the ONC distance is 450 pc, a luminosity of 2×10^{28} ergs s^{-1}. This is $\simeq 25$ times more sensitive than the *ROSAT* HRI study of the ONC (Gagné et al. 1995) and $\simeq 10$ times more sensitive than the *ROSAT* PSPC observation, which suffered considerable source confusion (Geier et al. 1995). For comparison, the emission of the contemporary Sun in the same X-ray band ranges from $\sim 2 \times 10^{25}$ ergs s^{-1} in its quiet phase to $\sim 1 \times 10^{28}$ ergs s^{-1} during its most violent flares (Peres et al. 2000). Note, however, that the conversion between count rate and luminosity will be much higher for stars that are heavily absorbed. Accurate luminosities for the entire sample require spectral analysis for each star, which is beyond the scope of the present paper.

To locate sources in a methodical fashion, we apply the source detection program WAVDETECT based on a Mexican hat wavelet decomposition and reconstruction of

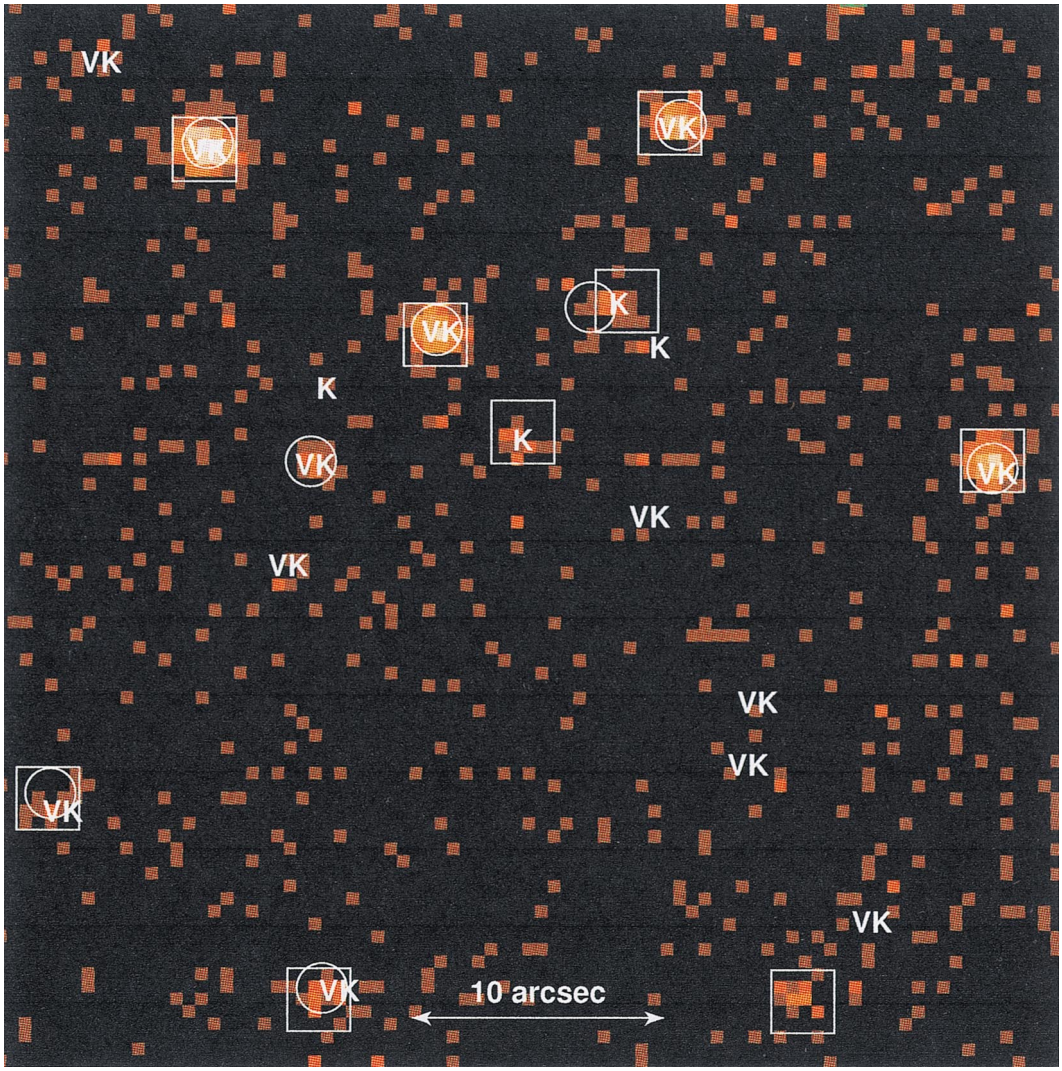

FIG. 2.—Expanded view of a typical small region at full resolution with 0.″5 × 0.″5 pixels. The background level is very low at $\simeq 0.08$ counts pixel^{-1}. The bright source near the western edge, Parenago 1959 ($V = 16.5$ K star), was the only source previously detected in this field (Gagné et al. 1995). White circles and squares show ACIS sources located with the wavelet detection algorithm in the soft and hard bands, respectively. "V" marks visible $V < 20$ stars (Hillenbrand 1997), and "K" near-infrared $K < 18$ stars (Hillenbrand et al. 1998; Hillenbrand & Carpenter 2000). The field is centered at $5^h35^m21^s.6$ $-5°22'12''$.

TABLE 1

ACIS SOURCES IN THE ONC

Source	R.A. (J2000.0)	Decl. (J2000.0)
Complete Sample (831):		
1	5 34 40.1	−5 26 43
2	5 34 41.6	−5 26 51
3	5 34 42.6	−5 28 35
4	5 34 44.4	−5 24 36
Additional Sources (142):		
832	5 34 40.8	−5 26 35
833	5 34 47.5	−5 28 16
834	5 34 48.2	−5 16 38
835	5 34 50.2	−5 29 13

NOTE.—Table 1 is presented in its entirety in the electronic edition of the Astronomical Journal. A portion is shown here for guidance regarding its form and content. Units of right ascension are hours, minutes, and seconds, and units of declination are degrees, arcminutes, and arcseconds.

the image (Freeman et al. 2000). We set the significance criterion at 1×10^{-5}, which permits a few false positive detections but gives good sensitivity. Wavelet scales between 1 and 16 pixels are used. The procedure is nearly complete to a limit of 7 photons near the field center increasing to 10 photons toward the edges of the field; many sources below these completeness limits are also located. A careful examination of the field by eye indicates the wavelet detection algorithm is quite reliable. The principal adjustments to the source lists were the removal of some dozens of spurious wavelet sources associated with the trails of the Trapezium sources and the addition of 19 sources just resolved (1″–3″ separation) from brighter sources. Source detection was performed separately in the soft (0.2–2 keV) and hard (2–8 keV) bands to improve sensitivity to unembedded and embedded sources respectively, after which the source lists were merged.

This procedure located 831 sources above the completeness limit and an additional 142 likely sources below this limit (Table 1). The sources should be designated CXOONC hhmmss.s-ddmmss, where the acronym stands for *Chandra X-Ray Observatory* Orion Nebula cluster. Source count rates range from 0.1 to >400 counts ks^{-1} (the lower limit here is due to loss of events because of photon pileup in θ^1C Ori), giving a very high dynamic range. This list of 973 ACIS sources was cross-correlated with a large catalog of $\simeq$2500 objects in the ONC and its vicinity including complete listings of 1578 stars with visible magnitude $V < 20$ (Hillenbrand 1997) and 854 stars from K-band surveys with limiting magnitude $K < 18$ in the central region (Hillenbrand et al. 1998; Hillenbrand & Carpenter 2000). We find that 860 of the 973 X-ray sources spatially coincide within 1″–2″ of V- or K-band cluster members. Systematic and statistical astrometric errors are <1″ (see § 5).

In addition to the optical-infrared stars, most of the known compact radio sources in the ONC region (Felli et al. 1993, and references therein) are detected in the ACIS image. These radio sources are a heterogeneous mixture of ionized stellar winds or nonthermal emission from both unobscured Trapezium O stars and embedded OB stars in the BN/KL region, magnetically active low mass PMS members, and sources without stellar counterparts, such as partially ionized globules within the giant Orion H II region (Garay 1987; Felli et al. 1993). We discuss some of these sources in § 5.

3. DEMOGRAPHICS OF X-RAY EMISSION IN THE ONC

Figure 2 illustrates several types of X-ray source identifications. The majority of the 973 X-ray sources are detected in both the soft and hard X-ray bands and are associated with relatively bright stars seen in the V and K surveys (*sources with circle, square, V and K*). Faint unobscured stars may be found only in the soft X-ray band (*circle, V and K*), while embedded stars are often seen only in the hard X-ray and K bands (*square and K*). Many of the fainter and more heavily absorbed ONC members, and a handful of unabsorbed stars, are not detected in X-rays (V and K or K alone).

One hundred and three ACIS sources found only in the hard band have no optical or infrared counterpart and are distributed approximately evenly across the ACIS field (square). Some of these are likely extragalactic sources, primarily active galactic nuclei, seen through the molecular cloud. Convolving the flux distribution of hard X-ray band source counts at high-Galactic latitudes (Ann Hornschemeier 2000, private communication; see Hornschemeier et al. 2000) with the distribution of hydrogen column densities across the ACIS field (estimated from a velocity-integrated $C^{18}O$ map using standard conversions to total column densities; John Bally 2000, private communication) predicts $\sim$25 hard extragalactic sources in the ACIS field. We conclude that most of the unidentified sources are ONC stars, probably faint embedded late-type PMS stars (§ 5). Others may be spurious due to flickering pixels.

Nine hundred and thirty four of the $V < 20$ stars are sufficiently well-characterized to be placed on the Hertzsprung-Russell (HR) diagram from which, together with theoretical evolutionary tracks (D'Antona & Mazzitelli 1997),[5] stellar masses and ages can be estimated (Hillenbrand 1997). Figure 3 shows this HR diagram with symbols coded for detection and nondetection in the ACIS image. The detection rate in the sample is 91% for stars with masses $M > 0.3\ M_\odot$ and 75% for stars with $0.1 < M < 0.3\ M_\odot$. The *Chandra* sensitivity of $\sim 2 \times 10^{28}$ ergs s^{-1} is thus sufficient to detect nearly all optically selected ONC stars with $V < 20$.

However, the V-band sample in the HR diagram systematically excludes the most obscured and least massive stars, particularly brown dwarfs, which are more effectively found at near-infrared wavelengths. Figure 4 compares the ACIS sources with the deep H and K band samples (Hillenbrand et al. 1998; Hillenbrand & Carpenter 2000). A strong relationship between X-ray detectability and K magnitude is present. Over 50% of cluster members with $M > 1\ M_\odot$ are detected, even if they suffered absorption as high as $A_V \simeq 60$, equivalent to a hydrogen column density $N_H \simeq 1 \times 10^{23}$ cm^{-2}. Stars between $0.1 < M < 1\ M_\odot$ are generally detected only if $A_V \leq 10$, and substellar objects with $M < 0.08\ M_\odot$ are rarely detected for any A_V. Astrophysical interpretation of these results is not simple because mass, luminosity, radius, reddening, and the effects of circumstellar disks are intertwined across the color-magnitude diagram. To remove the effect of obscuration, we restrict our examination to low-A_V stars having infrared colors $H-K < 0.5$. Again a strong relationship between ACIS detection fraction and K magnitude is found: the detection

[5] See also http://www.mporzio.astro.it/dantona.

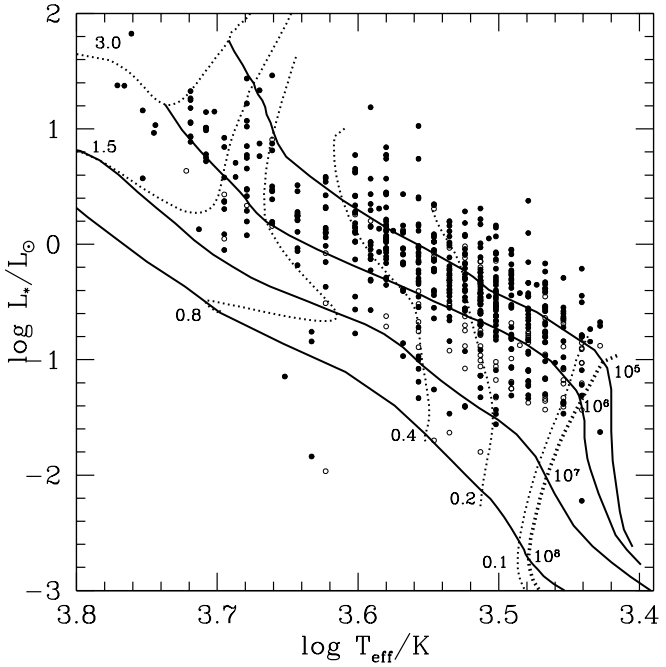

FIG. 3.—Hertzsprung-Russell diagram for well-characterized ONC stars with $V < 20$ in the ACIS field of view (Hillenbrand 1997). Filled circles indicate detections with ACIS and open circles indicate nondetections. Evolutionary tracks for stellar masses $M = 0.1, \ldots, 3.0\ M_\odot$ (*dotted curves*) and isochrones for ages $\log t = 5, \ldots, 8$ yr (*solid curves*) are from D'Antona & Mazzitelli (1997). Brown dwarfs lie below the dashed line at $M = 0.08\ M_\odot$.

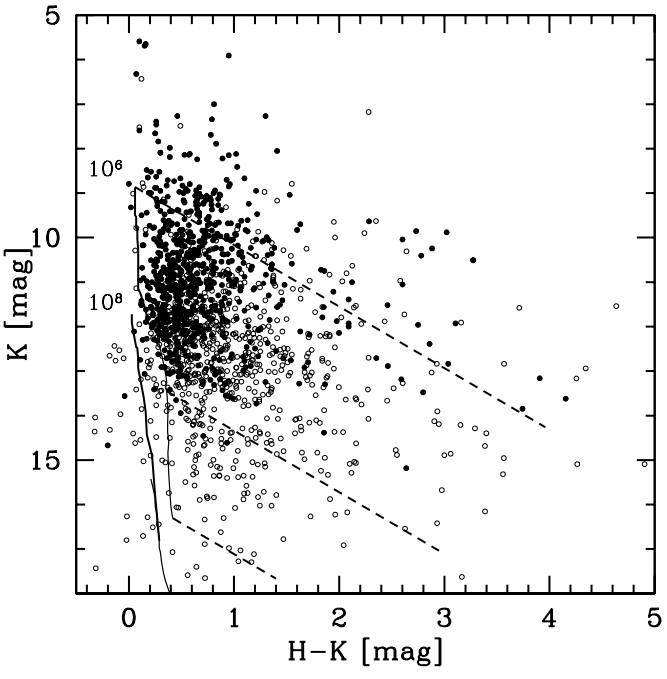

FIG. 4.—Near-infrared color-magnitude diagram for all objects with $K < 18$ in the ACIS field of view (Hillenbrand et al. 1998; Hillenbrand & Carpenter 2000). Filled circles are X-ray detections and open circles are nondetections. The vertical solid curves show the loci for unreddened stars with ages $\log t = 6,8$ yr. The dashed lines show the effects of reddening: $0 < A_V < 60$ for $M = 2.5\ M_\odot$ (*top*); $0 < A_V < 40$ for $M = 0.08\ M_\odot$ (*middle*); and $0 < A_V < 15$ for $M = 0.02\ M_\odot$ (*bottom*).

fraction declines from about 85% for $K < 11$ to about 50% for $11 \leq K < 13$, about 35% for $13 \leq K < 15$, and $< 8\%$ for $K > 15$.

A few of the 973 ACIS sources coincide with faint sources with inferred $M \simeq 0.05\ M_\odot$, assuming an age of 1 My (Figs. 3 and 4). These candidate PMS brown dwarfs are PC 116, PC 215, H 5096, HC 114, and HC 123 (Prosser et al. 1994; Hillenbrand & Carpenter 2000). Two of these have spectral type around M6–M7. Taken at face value, these brown dwarf candidates roughly double the number of PMS candidate brown dwarfs detected in the X-ray band at levels around 10^{28} ergs s^{-1} with the ROSAT satellite (Neuhäuser & Comerón 1998; Neuhäuser et al. 1999). However, because these ONC stars reside close to the $M = 0.08\ M_\odot$ line, infrared excesses from circumstellar disks may be present, photometric variability may occur, and theoretical models are uncertain; they may in fact evolve into hydrogen-burning stars. The strongest result from the ACIS ONC data is that great majority of PMS brown dwarfs found by Hillenbrand & Carpenter (2000) are not X-ray emitters with $L_x \gtrsim 2 \times 10^{28}$ ergs s^{-1}, our detection limit, in agreement with the *ROSAT* studies.

4. EVOLUTION OF X-RAY EMISSION IN SOLAR MASS STARS

Among solar-type *main-sequence* stars, it is well-established that X-ray emission arises from magnetic activity at the stellar surface, where the magnetic fields are generated by a magnetic dynamo in the stellar interior driven by rotation (Rosner, Golub, & Vaiana 1985). Thus, main-sequence stars show a correlation between L_x and surface rotational velocity, but little dependence between L_x and other stellar properties, such as bolometric luminosity $L_{\rm bol}$ or mass M. The situation for *pre–main-sequence* stars has been more confusing: despite considerable evidence that their X-ray emission is related to high levels of surface magnetic activity, L_x has been found to be strongly correlated with both $L_{\rm bol}$ and M (see e.g., Walter & Kuhi 1981; Feigelson et al. 1993; Casanova, Montmerle, & Feigelson 1995; Neuhäuser et al. 1995; Feigelson & Montmerle 1999). Furthermore, as PMS stars evolve downward in the Hertzsprung-Russell diagram during their early convective phases, a dependence on $L_{\rm bol}$ may mean that X-ray luminosity decreases with age t during PMS evolution. L_x may also scale with stellar radius (recall $R \propto L_{\rm bol}^{1/2}$ along vertical convective tracks) if reconnecting magnetic fields cover the entire surface of the star. A weak relation between L_x and stellar rotation is found in some but not all PMS samples.

These relationships have never been convincingly explained. If L_x–$L_{\rm bol}$, L_x–M, or $L_x - t$ correlations represent physical links, then PMS magnetic activity may not be based on the standard dynamo but rather on more exotic mechanisms. Such mechanisms include surface activity arising from magnetic fields inherited from the star formation processes rather than generated within the PMS stars, or violent reconnection events in magnetic fields connecting the star to the circumstellar disk (Feigelson & Montmerle 1999).

To untangle a part of this confusion, we consider only a narrow range of stellar masses around 1 $M_\odot$ to remove mass as a confounding variable. Figure 5 shows the plot of ACIS count rate versus bolometric luminosity for a complete sample of 17 ONC stars with $0.8 < M < 1.2\ M_\odot$ and low obscuration ($A_V < 3$). A well-defined sample of Pleiads

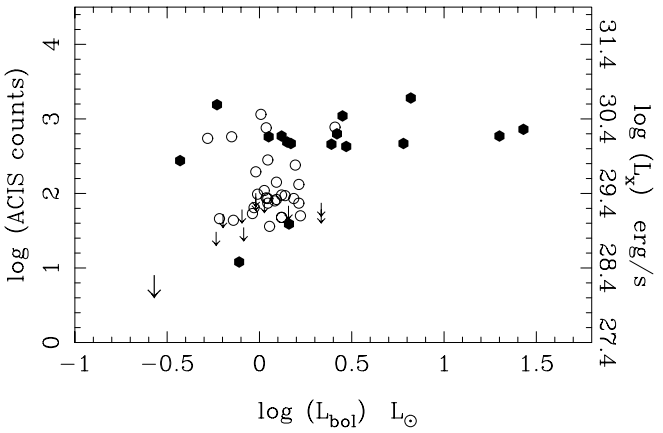

FIG. 5.—Scatter plot of ACIS counts in the soft (0.2–2 keV) band and bolometric luminosity for a complete sample of solar-mass ONC stars with $0.8 < M < 1.2\ M_\odot$ and $A_V < 3$ (*filled circles and large arrow*). The right axis gives an approximate conversion to soft X-ray luminosity assuming a $kT = 1$ keV thermal plasma. Zero-age main-sequence Pleiads in the same mass range are shown for comparison (*open circles and small arrows*).

in the same mass range observed with the *ROSAT* satellite, selected to have $0.52 \leq (B-V) \leq 0.74$, is shown for comparison (Stauffer et al. 1994; Micela et al. 1996). These studies established that rotational velocity is the dominant contributor to the wide dispersion in Pleiad X-ray emission.

Rather than a simple dependence between L_x and $L_{\rm bol}$, the X-ray emission of ONC solar-mass stars in Figure 5 might be divided into two epochs. During the first ~ 2 My as the bolometric luminosity fades by a factor of ~ 20, X-ray luminosities appear high and constant around $L_x \sim 2 \times 10^{30}$ ergs s^{-1}. This means the X-ray surface flux ($L_x/4\pi R^2$) increases as the star descends the Hayashi track, as found in *ROSAT* studies (Neuhäuser et al. 1995; Kastner et al. 1997). But as the stars age from ~ 2 to ~ 10 Myr and enter the radiative track, some stars retain their high X-ray levels while in others it drops by a factor of ~ 50 or more. The sample is small, so this pattern is not established with confidence.

This behavior is in accord with current views of a solar-type magnetic dynamo origin for PMS X-ray emission where rotation regulates the level of magnetic activity at the stellar surface and where rotation in turn is regulated by a magnetic coupling between the star and its circumstellar disk. In this model, the wide dispersion in L_x among older PMS stars reflects the wide dispersion in stellar rotation rates, which is expected from different durations of star-disk coupling (Bouvier et al. 1997). This same explanation accounts for the wide dispersion of L_x linked to stellar rotation found in zero-age main-sequence solar-mass Pleiades stars.

This dynamo interpretation of PMS X-ray emission can be directly tested using the sample shown in Figure 5: older ONC stars with high L_x (JW198, JW601, and JW738) should show faster rotational velocities in high-resolution optical spectra than those with low L_x (JW278, JW662, and JW868). If this prediction of the standard magnetic dynamo model is not validated in this and similar subsamples of the ONC, then nonsolar models for magnetic flaring in T Tauri stars must be considered.

5. X-RAYS FROM THE EMBEDDED BN/KL REGION

A cluster of embedded stars, including the $L_{\rm bol} \sim 10^4\ L_\odot$ Becklin-Neugebauer (BN) object lie near the density peak of the massive OMC-1 molecular cloud about 1′ northwest of the Trapezium (Genzel & Stutzki 1989). BN lies in a group of several $L_{\rm bol} \sim 10^3\ L_\odot$ massive stars (Gezari, Backman, & Werner 1998 and references therein), three of which (BN, IRc2, and infrared Source n) produce compact thermal radio sources (ultracompact H II regions and/or stellar winds) and/or maser outflows. This group of massive young stars illuminates the infrared Kleinman-Low (KL) nebula and powers strong shocked molecular outflows in the region (Stolovy et al. 1998 and references therein). BN/KL lies in the densest and most chemically rich region in the entire Orion giant molecular cloud complex, and it is the nearest and best-studied example of $\simeq 20$ known molecular hot cores, which are the likely sites of current massive star formation (Kurtz et al. 2000). The region is extremely complex and not fully understood after decades of intensive multiwavelength investigation.

To obtain a reliable detailed understanding of the X-ray emission in this crowded region, the ACIS data were specially processed for this analysis. First, we apply the software corrector for charge transfer inefficiency (§ 2) described by Townsley et al. (2000). This restores much of the degradation of event energies and grade distributions in a spatially dependent fashion across the CCD chip. Second, source detection proceeded as described in § 2. Third, source positions of several bright X-ray sources were matched to positions of infrared sources (aligned to the *Hipparcos* frame through the 2MASS survey; Hillenbrand & Carpenter 2000) and VLA radio sources (Felli et al. 1993; Menten & Reid 1995). A 0.″5 boresight correction was applied to the ACIS field resulting in a systematic astrometric accuracy better than $\pm 0.''1$ (estimated 90% confidence level). Individual source positions have estimated statistical uncertainties ranging from $\pm 0.''1$ for strong sources to $\pm 0.''5$ for weak sources (estimated 90% confidence).

Fourth, spectral analysis on the corrected data was performed with the XSPEC software package (Arnaud 1996). We present here the equivalent hydrogen column density associated with line-of-sight absorption. Due to uncertainties in the detector spectral response and the complexities of source spectra, we estimate the 90% confidence intervals to be ± 0.5 in $\log N_H$. Recall that $\log N_{\rm H} = 21.2$ cm^{-2} corresponds to $A_V = 1$ for normal elemental abundances and gas-to-dust ratios (Ryter 1996). Fifth, photon arrival times were tested for variability using a Kolmogorov-Smirnov one-sample test against a model of a constant source. We report source variations significant at the $P > 99.5\%$ confidence level.

Figure 6 shows a full-resolution view of the ACIS field around BN/KL in the 0.2–8 keV band. Unlike Figures 1 and 2, colors here represent the photon energy where red represents soft unabsorbed photons and blue represents hard photons. Twenty-seven sources above the limit of 7 photons (§ 2) found with wavelet detection and visual examination are indicated; their X-ray properties and counterparts are given in Table 2 and the Table notes. Two sources may be poorly resolved doubles with separations around 1.″5. Fainter sources are likely present; for example, a group of 5 photons around $(\Delta\alpha, \Delta\delta) = (12'', -16'')$ appears as a source in Table 1 and coincides with an anonymous $K \simeq 18$–19 NICMOS star (Stolovy et al. 1998).

In Table 2, running source numbers shown in Figure 6 are provided in column (1). X-ray centroid positions in

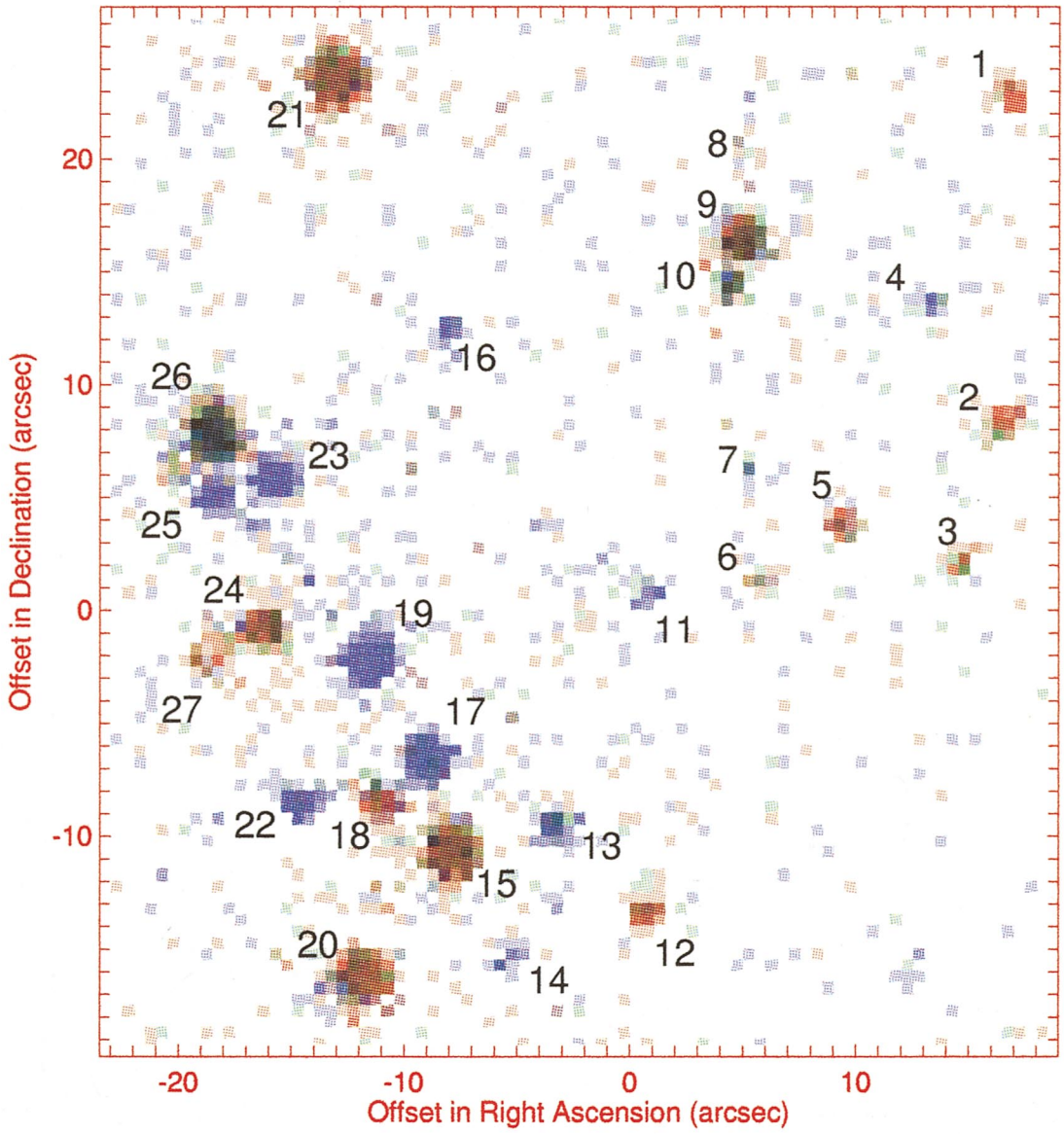

FIG. 6.—Expanded view of the Becklin-Neugebauer/Kleinman-Low region. In this figure, color hues are coded to X-ray energies of individual photons: red represents photons in the 0.5–1.5 keV band, green represent photons in the 1.5–2.5 keV band, and blue represents photons in the 2.5–8 keV band. Color intensity is scaled linearly to the number of photons in each pixel. Positions are indicated with respect to the Becklin-Neugebauer object. Table 2 gives source properties and counterparts.

columns (2)–(3) are in epoch J2000.0 from the ACIS image after boresight correction. Column (4) gives ACIS counts extracted from a 1.″5 circle in the 0.2–8 keV band with ASCA grades after correction for charge-transfer inefficiency. A background of 2 counts per source has been subtracted. Column densities rounded to the nearest dex (0.5) in column (5) are estimated from XSPEC fits to X-ray pulse height distributions. Column (6) provides offsets in arcseconds between the ACIS source and its counterpart, based on *K*-band (Hillenbrand & Carpenter 2000) or radio positions (Felli et al. 1993, adjusted to the astrometry of Menten & Reid 1995).

In column (7), we divide sources into three classes based on their counterparts: "ONC" ACIS sources are likely members of the Orion Nebula cluster, generally optically bright, lightly-absorbed stars; "IR" ACIS sources have infrared but not optical counterparts and are likely embedded young stars; and "X-ray" ACIS sources have no photospheric stellar counterparts. Columns (8)–(9) of Table 2 indicate the optical counterparts and magnitudes (Jones & Walker 1988 [JW]; Prosser et al. 1994 [PC]). Columns (10)–(11) give near-infrared counterparts and *K*-band magnitudes (JW; PC; Hillenbrand & Carpenter 2000 [HC]), except for magnitudes of BN and Source n obtained from Lonsdale et al. (1982). The final column points to notes on individual sources where optical counterpart information is from Hillenbrand (1997), infrared information is from Dougados et al. (1993), and radio information is from Felli et al. (1993), Menten & Reid (1995), and Menten (2000, private communication). X-ray variability and spectral properties are also summarized in the notes.

5.1. *Orion Nebula Cluster Members*

The majority of ACIS sources in the vicinity of BN are relatively unobscured ($A_V \lesssim 3$) members of the ONC, as

TABLE 2

ACIS Sources Near the Becklin-Neugebauer Object

ACIS Sources						Counterparts					
							Optical		Infrared		
No. (1)	R.A. (2)	Decl. (3)	Counts (4)	$\log N_H$ (cm $^{-2}$) (5)	θ (arcsec) (6)	Class (7)	ID (8)	I (9)	ID (10)	K (11)	Notes (12)
1.....	5 35 13.03	-5 22 00.8	35	21.5	0.2	ONC	JW395	15.3	HC544	12.3	[a]
2.....	5 35 13.05	-5 22 15.3	40	21.5	0.1	ONC	PC 029	14.2	HC505	11.0	[b]
3.....	5 35 13.17	-5 22 21.7	28	22.0	0.5	ONC	JW399ab	12.8	HC487	10.3	[c]
4.....	5 35 13.26	-5 22 10.0	16	22:	0.2	IR	...	...	HC523	12.8	
5.....	5 35 13.50	-5 22 19.6	36	21.5	0.3	ONC	JW411	13.5	HC495	10.3	[d]
6.....	5 35 13.75	-5 22 22.4	14	...	0.4	ONC	JW420	13.6	HC483	9.6	
7.....	5 35 13.77	-5 22 17.4	9	...	0.2	IR	...	...	HC499	11.0	[e]
8.....	5 35 13.79	-5 22 03.4	8	...	0.7	ONC	JW424	...	HC541	11.5	
9.....	5 35 13.80	-5 22 07.2	365	21.5	0.1	ONC	JW423	12.3	HC703	9.3	[f]
10.....	5 35 13.84	-5 22 09.2	59	22.0	0.2	IR	...	...	HC525	11.8	
11.....	5 35 14.06	-5 22 22.2	18	23.0	1.1	IR	...	...	BN	5.1	[g]
12.....	5 35 14.08	-5 22 37.1	53	21.5	0.5	ONC	JW432	13.0	HC438	9.8	[h]
13.....	5 35 14.35	-5 22 32.9	61	23.0	0.2	IR	...	...	Source n	10.1	[i]
14.....	5 35 14.50	-5 22 38.6	18	23.0	0.0	X-ray	...	...	...	...	[j]
15.....	5 35 14.66	-5 22 33.9	660	21.5	0.1	ONC	JW448	12.1	HC443	9.1	[k]
16.....	5 35 14.67	-5 22 11.4	21	23:	...	X-ray	...	...	...	...	[l]
17.....	5 35 14.73	-5 22 29.9	263	22.5	0.1	IR	...	...	HC464	10.5	[m]
18.....	5 35 14.88	-5 22 31.8	97	21.5	0.2	ONC	JW452	14.6	HC453	11.1	[n]
19.....	5 35 14.90	-5 22 25.6	426	23.0	0.1	X-ray	...	...	...	...	[o]
20.....	5 35 14.92	-5 22 39.4	574	21.5	0.2	ONC	JW454	11.9	HC431	...	[p]
21.....	5 35 14.99	-5 22 00.1	753	21.5	0.2	ONC	JW457	12.5	HC546	9.8	[q]
22.....	5 35 15.07	-5 22 31.3	62	23.5	0.5	ONC?	PC 086	15.6	HC456	12.0	[r]
23.....	5 35 15.17	-5 22 17.7	181	23.0	...	X-ray	...	...	...	...	[s]
24.....	5 35 15.21	-5 22 24.2	188	21.5	0.1	ONC	JW467	12.5	HC478	10.3	[t]
25.....	5 35 15.35	-5 22 18.4	75	23:	...	X-ray	...	...	...	...	[u]
26.....	5 35 15.35	-5 22 15.8	942	22.0	0.2	ONC	JW470	13.1	HC504	8.1	[v]
27.....	5 35 15.38	-5 22 25.7	34	21.0	0.3	ONC	JW472ab	12.9	HC475	10.1	[w]

[a] Optical ID: spectral type M2, $A_V = 4.7$, $L = 1.1\ L_\odot$, $M = 0.2\ M_\odot$, $\log t < 5$.
[b] ACIS morphology possibly double with separation 1.″5 along P.A. 135°. Optical ID = M4, $A_V = 0.4$, $L = 0.4\ L_\odot$, $M = 0.2\ M_\odot$, $\log t < 5$.
[c] Optical ID = K6.
[d] Optical ID = M1, $A_V = 1.3$, $L = 0.9\ L_\odot$, $M = 0.3\ M_\odot$, $\log t = 5$. Infrared ID = source e. Radio ID = faint 8.4 GHz radio source.
[e] Infrared ID = Source aa.
[f] Optical ID: K2, $A_V = 0.0$, $L = 1.3\ L_\odot$, $M = 0.2\ M_\odot$, $\log t < 5$. Infrared ID = Source g.
[g] Infrared ID = IRc1 = HC705. Radio ID = radio B. See text for discussion of possible positional offset.
[h] Optical ID: M3, $A_V = 1.8$, $L = 2\ L_\odot$, $M = 0.1\ M_\odot$, $\log t < 5$. Radio ID: = radio R.
[i] Infrared ID = HC448. Radio ID = double radio source with 0.″4 separation.
[j] Radio ID = radio H. The offset is with respect to the radio position. Possible infrared ID = IRc18 (10 μm) lies 1.″3 from the ACIS source Gezari et al. 1998.
[k] Optical ID = K7, $A_V = 2.3$, $L = 5\ L_\odot$, $M = 0.3\ M_\odot$, $\log t < 5$. Infrared ID = Source t. Radio ID = faint 8.4 GHz radio source.
[l] Radio ID = faint 8.4 GHz radio source.
[m] ACIS count rate drops then rises by factor $\simeq 2$ in $\simeq 5$ hr. Optical ID = double with HC465, $V = 10.5$.
[n] ACIS count rate rises, falls and rises again over the entire 13 hr observation.
[o] ACIS count rate shows slow rise and fall in count rate over 13 hr observation with factor $\simeq 2$ amplitude. Radio ID = radio D. The offset is with respect to the radio position.
[p] Optical ID = MS-16. K4, $A_V = 2.3$, $L = 6\ L_\odot$, $M = 0.8\ M_\odot$, $\log t = 5$.
[q] ACIS count rate drops by factor of $\simeq 2$ in $\simeq 5$ hr. Optical ID = K3, $A_V = 2.0$, $L = 3\ L_\odot$, $M = 0.8\ M_\odot$, $\log t < 5$.
[r] ACIS count rate decreases after $\simeq 3$ hr. Optical ID = M6, $A_V = 0.6$, $L = 0.2\ L_\odot$, $M = 0.1\ M_\odot$, $\log t < 5$. See text for discussion of the uncertain counterpart of this X-ray source.
[s] ACIS spectrum is unusually hard out to 7 keV.
[t] Optical ID = K7, $A_V = 1.4$, $L = 1\ L_\odot$, $M = 0.4\ M_\odot$, $\log t = 5.6$.
[u] ACIS count rate drops by factor of $\simeq 2$ in $\simeq 1$ hr, then falls again $\simeq 10$ hr later. ACIS spectrum is unusually hard out to 7 keV.
[v] ACIS count rate shows slow decline for $\simeq 10$ hr, followed by rise and fall (flare?) by a factor of $\simeq 2$ within $\simeq 2$ hr. Optical ID = mid-K.
[w] ACIS morphology is possibly double with separation 1.″5 along P.A. 120°.

expected given the proximity ($\simeq 1'$ or $\simeq 0.1$ pc) to the Trapezium. The X-ray stars are very young with estimated ages below 1 Myr. Most are lower mass stars with $M \simeq 0.1$–$0.4\ M_\odot$, although two X-ray bright $0.8\ M_\odot$ stars are present. The poorly studied late-K star JW 470 = CXOONC J053515.3−052215 is the most magnetically active star of this class, exhibiting the strongest and most variable X-ray emission. The identification of CXOONC J053515.0−052231 with the unobscured optical star PC 086 is uncertain despite the 0.″5 spatial coincidence, as the X-ray source appears heavily absorbed while the optical star is not. An alternative possible counterpart is the 12.4 μm source IRc14 lying 2.″0 from the X-ray location (Gezari et al. 1998).

Two ACIS sources in this class, CXOONC J53514.0−052237 = JW 432 and CXOONC J053514.6−052233

= JW 448, are radio sources. These and other radio sources discussed here are generally variable and are classified as FOXES, fluctuating optical and X-ray emitting sources, by Garay (1987). They resemble the several dozen known weak-lined T Tauri stars seen in nearby star-forming regions exhibiting nonthermal gyrosynchrotron radio emission and strong X-ray emission (André 1996; Feigelson & Montmerle 1999). These radio/X-ray ONC stars have probably lost their interacting disks at a very young age, resulting in rapid rotation and high levels of magnetic flaring.

5.2. *Embedded Infrared Stars*

Six ACIS sources are associated with embedded 2 μm stars without visible counterparts. Four of these are consistent with embedded but otherwise ordinary low-mass ONC members. CXOONC J053514.3−052232, however, coincides with the luminous infrared Source n. This $L_{\rm bol} \simeq 10^2$ $L_\odot$ member of the BN/KL group lies at the center of the dense molecular hot core and a H_2O maser outflow, and it appears to be associated with both a nonthermal double radio source and diffuse thermal radio emission (Menten & Reid 1995; Chandler & Wood 1997; Gezari et al. 1998). The unabsorbed X-ray luminosity of order 10^{30}–10^{31} ergs s^{-1} is consistent with a magnetically active low-mass protostar or T Tauri star or with an ordinary early-type B star.

Perhaps most remarkable among these sources is CXOONC J053514.0−052222, which lies 1.″1 northwest of the BN object itself. This offset appears larger than the expected positional uncertainties, estimated at $\pm 0.''5$ at 90% confidence. But only $\simeq 18$ source photons are present and we cannot be completely confident the offset is real. One possibility is that the X-ray source is unrelated to the BN object but arises from an uncataloged embedded ONC star; the energy distribution of the detected X-ray photons suggests $A_V \sim 50$. Another possibility is that the emission arises from outflows from the BN object. The photon distribution is consistent with a source structure $\lesssim 1''(\simeq 500$ AU) in extent. Hydrodynamical calculations of ultracompact H II regions with mass-loaded winds from massive young stars pushing into a stationary dense medium indicate that, although the emission is dominated by readily absorbed ultraviolet photons, some high-energy X-rays are produced and escape from the immediate environment (Strickland & Stevens 1998, see also Arthur, Dyson, & Hartquist 1993). There are also possibilities of nonequilibrium shock processes giving rise to X-ray emission at the interfaces between H II regions and molecular material (Dorland & Montmerle 1987).

5.3. *X-Ray Sources without Optical or Infrared Counterparts*

The five ACIS sources in the "X-ray" class have no photospheric counterparts in the deepest available optical, K band, and mid-infrared surveys of the region (Stolovy et al. 1998; Hillenbrand & Carpenter 2000; Gezari et al. 1998). All five sources are heavily absorbed with $\log N_H \simeq 23$ cm^{-2} or roughly $A_V \sim 50$, two exhibit short-timescale X-ray variability, and three are associated with compact, likely variable radio sources (Felli et al. 1993). The two ACIS sources not associated with radio sources have unusually hard X-ray spectra similar to those seen in Class I protostars and T Tauri stars during powerful flares (Koyama et al. 1996; Tsuboi et al. 1998). CXC J053514.9−052225 = radio D is the most extreme of these sources. Its luminosity would be $L_x \simeq 10^{31}$ ergs s^{-1} if it were unobscured.

Three explanations for these sources might be considered: background Galactic or extragalactic sources unrelated to the Orion star forming region, X-ray luminous low-mass protostars (one of the dozen known X-ray emitting Class I protostars is a nonthermal radio variable; Feigelson et al. 1998), or magnetically active low-mass radio-loud (i.e., weak-lined T Tauri) stars. We estimate that only 0–1 of these six sources may be an extragalactic object seen through the molecular cloud (§ 3). Protostars are possible, but perhaps their disks or outflows should have been detected in the extensive infrared and molecular studies of the region. We suggest that the third alternative is most plausible. The X-ray and radio properties are consistent with deeply embedded low-mass PMS stars having unusually high $L_x/L_{\rm bol}$ ratios, such that their photospheric emission falls below current infrared sensitivity limits ($K \simeq 19$; Stolovy et al. 1998).

It is worth remarking on the absence of certain objects in BN/KL region. The failure to detect the widely discussed multiple infrared sources comprising IRc2 (Dougados et al. 1993) could be due to their high level of absorption ($A_V \simeq 58$; Gezari et al. 1998). No extended emission is evident in this portion of the ACIS image. X-rays are thus not detected from infrared-luminous dust condensations (IRc3, IRc4, IRc7, infrared shell or crescent; Stolovy et al. 1998), or the molecular hot core, plateau, or H_2 outflows (see e.g., Wright, Plambeck, & Wilner 1996). A recent supernova explosion in the region (Kundt & Yar 1997) is clearly excluded by the low background level seen in Figure 6.

Independent of the nature of the host stars, a clear astrophysical implication of the X-ray emission from deeply embedded PMS stars in the BN/KL region and the wider ONC field is that X-ray dissociation regions (Hollenbach & Tielens 1997) will be present even in the densest molecular cloud cores. These are volumes around X-ray emitting PMS stars where X-ray ionization dominates cosmic-ray ionization. X-ray irradiation on molecular cloud interiors is predicted to have a variety of effects on the dynamics, astrochemistry, and dust characteristics of molecular material (Glassgold, Feigelson, & Montmerle 2000), although little evidence for such effects has yet been found.

6. CONCLUSIONS

A 48 ks *Chandra* ACIS image of the Orion Nebula in the 0.2–8 keV band with a limiting sensitivity of $\simeq 2 \times 10^{28}$ ergs s^{-1}, arcsecond spatial resolution, and subastrometric precision reveals as follows:

1. About 1000 X-ray sources are associated with magnetically active pre–main-sequence stars in the Orion Nebula Cluster. Almost 90% of the visible stars with $V < 20$ are detected across the entire Hertzsprung-Russell diagram. Higher mass stars are detected even when subject to tens of magnitudes of absorption, while the lowest mass stars and substellar objects are typically not detected.

2. The relationships between X-ray emission and other stellar properties are complex and should be elucidated in a more complete analysis of the ONC. Examination of a well-defined subsample of solar mass stars suggests a high constant X-ray luminosity around 2×10^{30} ergs s^{-1}, hence increasing surface flux, as stars descend the convective

Hayashi track followed by an increased dispersion in X-ray luminosities as they enter the radiative track. The suggested interpretation, that this dispersion in magnetic activity is due to different rotational evolutions of different stars, can be easily tested with measurements of stellar rotational velocities. These results may be relevant to the evolution of magnetic activity in the early Sun.

3. A close examination of X-ray sources in the BN/KL region of OMC 1 shows a diversity of stellar sources: foreground and embedded ONC members; the luminous embedded infrared Source n; several sources not appearing in sensitive optical and K-band surveys; and a faint, heavily absorbed source apparently displaced 1″ from BN itself. The X-ray spectra indicate line-of-sight absorption ranging from $21 \lesssim \log N_{\rm H} \lesssim 23$ cm^{-2} and one-fourth of the sources are variable within the observation. A considerable fraction of the sources are associated with faint radio sources; this likely arises from nonthermal gyrosynchrotron radiation that accompanies X-ray flaring induced by magnetic reconnection. The ACIS source associated with Source n may be the first unambiguous (i.e., spatially resolved from other young stars) X-ray detection of a massive young stellar object. The X-ray source near BN is enigmatic. It is unclear whether it is a separate star or whether the X-rays are produced in the outflow from this massive young star. The several sources without any photospheric optical or infrared counterpart are likely new embedded, magnetically active stars in OMC 1. The presence of deeply embedded X-ray sources in the BN/KL region support the idea that ionizing X-rays produced by young stars will be present within dense star-forming molecular cloud cores.

We express our appreciation of the many scientists and engineers who brought *Chandra* to fruition, in particular those at MIT, Penn State, and Lockheed-Martin who contributed to the ACIS instrument. Ann Hornschemeier (Penn State), Karl Menten (MPI-Radioastronomie), and John Bally (Colorado) kindly provided results prior to publication, and the referee Ralph Neuhäuser gave many useful comments. This research was funded by NASA contract NAS 8-38252 at Penn State. The contributions of S. H. P. were carried out at the Jet Propulsion Laboratory, California Institute of Technology, under contract with the National Aeronautics and Space Administration.

REFERENCES

Alcalá, J. M., et al. 1996, A&AS, 119, 7
André, P. 1996, in ASP Conf. Ser. 93, Radio Emission from the Stars and the Sun, ed. A. R. Taylor & J. M. Paredes (San Francisco: ASP), 273
Arnaud, K. A. 1996, in ASP Conf. Ser. 101, Data Analysis Software and Systems V, ed. G. H. Jacoby & J. Barnes (San Francisco: ASP), 17
Arthur, A. S., Dyson, J. S., & Hartquist, T. W. 1993, MNRAS, 261, 425
Bouvier, J., Forestini, M., & Allain, S. 1997, A&A, 326, 1023
Bradt, H. V., & Kelley, R. L. 1979, ApJ, 228, L33
Casanova, S., Montmerle, T., & Feigelson, E. D. 1995, ApJ, 439, 752
Chandler, C. J., & Wood, D. O. S. 1997, MNRAS, 287, 445
Churchwell, E. 1999, in The Origin of Stars and Planetary Systems, ed. C. J. Lada & N. D. Kylafis (Dordrecht: Kluwer), 515
D'Antona, F., & Mazzitelli, I. 1997, Mem. Soc. Astron. Italiana, 68, 807
den Boggende, A. J. F., Mewe, R., Gronenschild, E. H. B. M., Heise, J., & Grindlay, J. E. 1978, A&A, 62, 1
Dorland, H., & Montmerle, T. 1987, A&A, 177, 243
Dougados, C., Léna, P., Ridgway, S. T., Christou, J. C., & Probst, R. G. 1993, ApJ, 406, 112
Feigelson, E. D., Carkner, L., & Wilking, B. A. 1998, ApJ, 494, L215
Feigelson, E. D., Casanova, S., Montmerle, T., & Guibert, J. 1993, ApJ, 416, 623
Feigelson, E. D., & Montmerle, T. 1999, ARA&A, 37, 363
Feigelson, E. D., et al. 2000, in preparation
Felli, M., Taylor, G. B., Catarzi, M., Churchwell, E., & Kurtz, S. 1993, A&AS, 101, 127
Freeman, P. E., Kashyap, V., Rosner, R., & Lamb, D. Q. 2000, ApJ, submitted
Gagné, M., Caillault, J.-P. & Stauffer, J. R. 1995, ApJ, 445, 280
Garmire, G., et al. 2000, in prepartion
Garay, G. 1987, Rev. Mexicana Astron. Astrofis., 14, 489
Geier, S., Wendker, H. J., & Wisotzki, L. 1995, A&A, 299, 39
Genzel, R., & Stutzki, J. 1989, ARA&A, 27, 41
Gezari, D. Y., Backman, D. E., & Werner, M. W. 1998, ApJ, 509, 283
Giacconi, R., Murray, S., Gursky, H., Schreier, E., & Tananbaum, H. 1972, ApJ, 178, 281
Glassgold, A. E., Feigelson, E. D., & Montmerle, T. 2000, in Protostars and Planets IV, ed. V. Mannings et al. (Tucson: Univ. Arizona Press), 429
Hillenbrand, L. A. 1997, AJ, 113, 1733
Hillenbrand, L. A., & Carpenter, J. 2000, ApJ, in press
Hillenbrand, L. A., Strom, S. E., Calvet, N., Merrill, K. M., Gatley, I., Makidon, R. B., Meyer, M. R., & Skrutskie, M. F. 1998, AJ, 116, 1816
Hollenbach, D. J., & Tielens, A. G. G. M. 1997, ARA&A, 35, 179
Hornschemeier, A., et al. 2000, ApJ, in press
Jones, B. F., & Walker, M. F. 1988, AJ, 95, 1755
Kastner, J. H., Zuckerman, B., Weintraub, D. A., & Forveille, T. 1997, Science, 277, 67
Koyama, K., Ueno, S., Kobayashi, N., & Feigelson, E. D. 1996, PASJ, 48, L87
Ku, W. H.-M. & Chanan, G. A. 1979, ApJ, 234, L59
Kundt, W., & Yar, A. 1997, Ap&SS, 254, 1
Kurtz, S., Cesaroni, R., Churchwell, E., Hofner, R. & Walmsley, M. 2000, in Protostars and Planets IV, ed. V. Mannings et al. (Tucson: Univ. Arizona Press), 299
Lonsdale, C. J., Becklin, E. E., Lee, T. J., & Stewart, J. M. 1982, AJ, 87, 1819
Menten, K. M., & Reid, M. J. 1995, ApJ, 445, L157
Micela, G., Sciortino, S., Kashyap, V., Harnden, F. R., Jr., & Rosner, R. 1996, ApJS, 102, 75
Neuhäuser, R. & Comerón, F. 1998, Science, 282, 83
Neuhäuser, R., Sterzik, M. F., Schmitt, J. H. M. M., Wichmann, R., & Krautter, J. 1995, A&A, 297, 391
Peres, G., Orlando, S., Reale, F., Rosner, R., & Hudson, H. 2000, ApJ, 528, 537
Preibisch, T. 1997, A&A, 320, 525
Prigozhin, G., Kissell, S., Bautz, M., Grant, C., LaMarr, B., Foster, R., & Ricker, G. 2000, Proc. SPIE, 4012, in press
Prosser, C. F., Stauffer, J. R., Hartmann, L., Soderblom, D. R., Jones, B. F., Werner, M. W., & McCaughrean, M. J. 1994, ApJ, 421, 517
Rosner, R., Golub, L., & Vaiana, G. S. 1985, ARA&A, 23, 413
Ryter, C. E. 1996, Ap&SS, 236, 285
Stauffer, J. R., Caillault, J.-P., Gagné, M., Prosser, C. F., & Hartmann, L. W. 1994, ApJS, 91, 625
Stolovy, S. R., et al. 1998, ApJ, 492, L151
Strickland, D. K., & Stevens, I. R. 1998, MNRAS, 297, 747
Townsley, L., Broos, P., Garmire, G., & Nousek, J. 2000, ApJ, 534, L139
Tsuboi, Y., Koyama, K., Murakami, H., Hayashi, M., Skinner, S., & Ueno, S. 1998, ApJ, 503, 894
Walter, F. M., & Kuhi, L. V. 1981, ApJ, 250, 254
Weisskopf, M. C., O'Dell, S. L., & van Speybroeck, L. P. 1996, Proc. SPIE, 2805, 2
Wright, M. C. H., Plambeck, R. L., & Wilner, D. J. 1996, ApJ, 469, 216
Yamauchi, S., Koyama, K., Sakano, M., & Okada, K. 1996, PASJ, 48, 719